Sequential Observations of Flux Transfer Events, Poleward-Moving Auroral Forms, and Polar Cap Patches

K.-J. Hwang[1] , Y. Nishimura[2] , A. J. Coster[3] , R. G. Gillies[4] , R. C. Fear[5] , S. A. Fuselier[1] , S. M. Petrinec[6] , J. L. Burch[1] , K. Dokgo[1] , D. G. Sibeck[7] , B. L. Giles[7] , C. T. Russell[8] , R. J. Strangeway[8] , D. J. Gershman[7] , C. J. Pollock[9] , Y. Khotyaintsev[10] , R. B. Torbert[11] , R. E. Ergun[12] , J. I. Moen[13] , and L. B. Clausen[13]

[1]Southwest Research Institute, San Antonio, TX, USA, [2]Electrical and Computer Engineering and Center for Space Physics, Boston University, Boston, MA, USA, [3]Haystack Observatory, MIT, Boston, MA, USA, [4]Physics & Astronomy, University of Calgary, Calgary, Alberta, Canada, [5]School of Physics and Astronomy, University of Southampton, Southampton, UK, [6]Lockheed Martin Advanced Technology Center, Palo Alto, CA, USA, [7]NASA Goddard Space Flight Center, Greenbelt, MD, USA, [8]Institute of Geophysics and Planetary Physics, University of California, Los Angeles, Los Angeles, CA, USA, [9]Denali Scientific, LLC, Fairbanks, AK, USA, [10]Swedish Institute of Space Physics, Uppsala, Sweden, [11]Space Science Center, University of New Hampshire, Durham, NH, USA, [12]Laboratory for Atmospheric and Space Physics, University of Colorado at Boulder, Boulder, CO, USA, [13]Department of Physics, University of Oslo, Oslo, Norway

Abstract We report the observation of solar wind-magnetosphere-ionosphere interactions using a series of flux transfer events (FTEs) observed by Magnetospheric MultiScale (MMS) mission located near the dayside magnetopause on 18 December 2017. The FTEs were observed to propagate duskward and either southward or slightly northward, as predicted under duskward and southward interplanetary magnetic field (IMF). The Cooling model also predicted a significant dawnward propagation of northward-moving FTEs. Near the MMS footprint, a series of poleward-moving auroral forms (PMAFs) occurred almost simultaneously with those FTEs. They propagated poleward and westward, consistent with the modeled FTE propagation. The intervals between FTEs, relatively consistent with those between PMAFs, strongly suggest a one-to-one correspondence between the dayside transients and ionospheric responses. The FTEs embedded in continuous reconnection observed by MMS and corresponding PMAFs individually occurred during persistent auroral activity recorded by an all-sky imager strongly indicate that those FTEs/PMAFs resulted from the temporal modulation of the reconnection rate during continuous reconnection. With the decay of the PMAFs associated with the FTEs, patch-like plasma density enhancements were detected to form and propagate poleward and then dawnward. Propagation to the dawn was also suggested by the Super Dual Auroral Radar Network (SuperDARN) convection and Global Positioning System (GPS) total electron content data. We relate the temporal variation of the driving solar-wind and magnetospheric mechanism to that of the high-latitude and polar ionospheric responses and estimate the response time.

Plain Language Summary The solar wind-magnetosphere coupling often occurs in a nonsteady manner. Such disturbances modify the magnetosphere-ionosphere system. One of the most common/important processes of such nonsteady phenomena is time-dependent dayside reconnection, as observationally evidenced by flux transfer events (FTEs), which have been, in turn, represented by ionospheric poleward-moving auroral forms (PMAFs). Decaying PMAFs have, then, been followed by the occurrence of polar cap patches, which are regions of plasma density enhancements observed in the polar cap. This study indicates a sequence of dynamic processes from the driving solar wind, nonsteady reconnection/FTEs, PMAFs, and polar cap patches. Although a portion of this link has been studied and reported, the complete sequence of these connections and full picture of the solar wind-magnetopause-ionosphere coupling have rarely been reported and examined. The series of FTEs embedded in continuous reconnection and corresponding PMAFs individually occurred during persistent auroral activity strongly indicate that the FTEs and PMAFs were in response to the temporal modulation of the reconnection rate during continuous reconnection, rather than the repeated, complete turn-on and turnoff of dayside reconnection. Our study advances the knowledge of Magnetosphere-Ionosphere-Coupling near the cusp region and in the open field-line region that has been less developed than on closed field lines.

1. Introduction

The Dungey cycle (Dungey, 1961) refers to the dynamics of transport of mass, momentum, and energy from the solar wind into the Earth's magnetosphere, via the opening of the magnetic field lines at the dayside subsolar magnetopause, antisunward convection of these open flux tubes swept by the magnetosheath flow and reclosing of the magnetic field lines in the nightside magnetotail. Contrary to this large-scale and quasi-steady driving, the solar wind-magnetosphere coupling often occurs in a localized and nonsteady or transient manner, and such disturbances modify the responses of the magnetosphere-ionosphere system.

Among various types of transient phenomena responsible for the solar wind-magnetosphere-ionosphere interactions, one of the most common and important processes is transient dayside reconnection. Its observational evidence was identified as spacecraft crossing of a single structure or a series of bipolar signatures in the magnetic field component normal to the magnetopause (B_n). Russell and Elphic (1978) first termed this signature a flux transfer event (FTE). Typical signatures of FTEs, in addition to the B_n reversal, include enhanced magnetic field strength (B) due to a strong core field, an increase in the total pressure at the center, and a mixture of the magnetosphere or the magnetosheath plasmas. These signatures have been explained by their generation via (1) transient bursts of dayside reconnection (Russell & Elphic, 1978), (2) the complete turn-on and turnoff of single X-line reconnection (Scholer, 1988; Southwood et al., 1988), (3) temporal modulation of the reconnection rate during continuous single X-line reconnection (Phan et al., 2004), or (4) multiple X-line reconnection (Lee & Fu, 1985; Scholer, 1995). The different (while evoking the common nonsteady nature of dayside reconnection) generation mechanisms give rise to different magnetic field topology and connectivity within/around the FTE, which have been detailed by recent observations by Magnetospheric MultiScale (MMS) mission (Burch et al., 2016; Hwang et al., 2016, 2017, 2018, 2020; Kacem et al., 2018).

The signatures of FTEs are, in turn, displayed in the ionosphere at their footprints of newly opened magnetic field lines. These signatures have been observed (1) by all-sky image (ASI) cameras as poleward-moving auroral forms (PMAFs; Fasel, 1995; Fasel et al., 1992; Sandholt et al., 1986) and (2) by radar as pulsed ionospheric flows (PIFs; McWilliams et al., 2000; Milan et al., 1999; Pinnock et al., 1993, 1995; Provan et al., 1999; Provan & Yeoman, 1999; Rae et al., 2004). Conjugate studies between spacecraft crossing the magnetopause and ionospheric signatures of FTEs (Amm et al., 2005; Elphic et al., 1990; McWilliams et al., 2004; Wild et al., 2001, 2003, 2005, 2007; Zhang et al., 2010) have shown the link. In particular, Neudegg et al. (2001) reported simultaneous observations of FTE signatures using the data from the Equator-S spacecraft on a geostationary orbit, the Polar spacecraft's Visible Imaging System (VIS) Camera, and the Super Dual Auroral Radar Network (SuperDARN). Noting ~2- to 3-min Alfvén transit time, that is, the time delay for the effects of reconnection to propagate from the dayside reconnection site to the ionosphere at the Alfvén speed along geomagnetic field lines (and the similar time delay for the FTE-associated magnetic-field disturbances to propagate from the subsolar magnetopause to Equator-S), Neudegg et al. (2000, 2001) showed that the difficulty sometimes presents in finding one-to-one correspondence between in situ FTE observations and ionospheric counterparts, while the majority (64–77%) of their statistics exhibit the correlation. Both FTEs and PMAFs occur azimuthally localized (Lockwood et al., 1989; Sandholt et al., 2003; Walsh et al., 2017). The extent and spreading of PMAFs can provide information related to the magnetopause reconnection X-line that are hard to determine mostly due to the constraint in observing the large-scale dayside magnetopause behavior beyond satellite locations.

These ionospheric flows associated with FTEs, after initiating around the dayside cusp region, propagate antisunward/poleward before fading away (Lorentzen et al., 2010). The average lifetime of PMAFs is ~10 min, and their latitudinal transit range is ~5° (Drury et al., 2003; Wang et al., 2016 and references therein). Such transient plasma flows have been related to localized structures of enhanced F-region plasma density (Goodwin et al., 2015). In particular, injection across the cusp into the polar cap and propagation over the polar cap of those structures, so-called polar cap patches, have been found to be associated with decaying of PMAFs (Carlson et al., 2004, 2006; Lorentzen et al., 2010).

Polar cap patches, referred to as plasma density anomalies with densities at least double those of the surrounding background plasma (Crowley, 1996; Weber & Buchau, 1981), have been identified as (1) 630.0-nm wavelength emissions by ASI cameras (resulting from recombination between electrons and molecular oxygen ions), (2) high-frequency backscatter power by radars or electron density measurements by

incoherent scatter radars and ionosondes, (3) enhanced total electron content (TEC) measurements by Global Positioning System (GPS) receivers (Clausen et al., 2016), or (4) plasma density irregularities by in situ satellites or sounding rockets. They are typically formed as cigar-shaped islands of F-region plasma (with ~500–1,000 km east/west width and ~100 s km thickness along the noon-midnight meridian). The midlatitude ionospheric plasma locally produced by solar extreme ultraviolet (EUV) radiation is thought to serve as a reservoir of source plasma for polar cap patches (Carlson, 2012; Foster, 1984; Knudsen, 1974). Focused studies over the last decade have been made to understand how the high-density solar EUV-ionized plasma can be entrained from the subauroral latitudes through the cusp dayside auroral region into the polar cap in the form of segmented islands. A frequently cited mechanism for southward interplanetary magnetic fields (IMFs) is transient dayside reconnection (figure 4 of Lockwood & Carlson, 1992; Carlson et al., 2004). The key processes include the initial equatorward expansion of the open-closed boundary, the poleward enhancement of the plasma flow by the reconnection potential, an equatorward jump of the X line, and the resulting poleward motion of a high-density plasma boundary. Some patches have been found to propagate across the entire polar cap from the dayside cusp to the nightside auroral oval and interact with nightside aurora (Nishimura et al., 2014).

These studies indicate a sequence of dynamic processes from the driving solar wind (southward IMF), nonsteady dayside reconnection/FTEs, PMAFs, and polar cap patches. Although a portion of this link has been widely studied and reported, the complete sequence of these connections and full picture of the solar wind-dayside magnetopause-ionosphere coupling have rarely been reported and examined.

In this paper, we use the data from Acceleration, Reconnection, Turbulence, and Electrodynamics of Moon's Interaction with the Sun (ARTEMIS; for solar wind inputs), MMS (for dayside dynamics), ASI cameras (for PMAFs), radars, and GPS (for polar cap patches and their propagation) to reveal the complete sequence. Using the nonsteady event occurred on 18 December 2017, we relate the temporal variation of the driving solar wind and magnetospheric mechanism to that of the high-latitude and polar ionospheric responses and estimate the response time. Our study advances the knowledge of Magnetosphere-Ionosphere-Coupling near the cusp region and in the open field line region that has been less developed than on closed field lines.

The following section briefly describes the data and instruments used for the present study. An overview of the event including MMS observations of the dayside magnetopause and boundary layer and ARTEMIS measurements of solar wind conditions as well as analysis of a series of FTEs is shown in section 3. The spatiotemporal properties of dayside reconnection inferred from MMS observations are analyzed in section 4. We then discuss ASI of the northern high-latitude and polar region that shows PMAFs associated with the FTEs passed by MMS, comparing their spatiotemporal variation in section 5, where we also investigate GPS detection of a weak signature of polar cap patches that arise following the decaying/weakening of the PMAFs and their propagation identified by GPS and radar. Discussion and conclusions of the comprehensive link of the solar wind, dayside magnetosphere, and ionosphere interaction follow in section 6.

2. Instrumentation

The four MMS spacecraft (Burch et al., 2016) fly in almost equatorial orbits in a tetrahedral configuration. Their identically equipped instruments include fluxgate magnetometers (FGMs) (Russell et al., 2014), Fast Plasma Investigation (FPIs) (Pollock et al., 2016), and Hot Plasma Composition Analyzer (HPCA; Young et al., 2014). The magnetic field data obtained from FGM have a time resolution of 10 ms in burst mode. The particle data from FPI provide plasma moments and 3-D distributions of ions and electrons over an energy range from 10 eV to 26 keV in 150 ms (for ions) and 30 ms (electrons) in burst mode. The ion mass spectrometer, HPCA, measures ion composition with 3-D distributions of five major ion species from 1 eV to 40 keV at a 10-s time resolution.

The Moon-orbiting ARTEMIS spacecraft (Angelopoulos, 2011), designed to investigate the Moon's interaction with the solar wind, provide high-resolution data of solar wind conditions. We use the data from the FGM and electrostatic analyzer (ESA) to obtain IMF orientation, plasma density, and pressures.

ASIs provide the two-dimensional display of the ionospheric phenomena as emissions often in the 630.0- and 557.7-nm wavelength above 20° elevation at 30-s temporal resolution (Moen et al., 2012). For the present event, we use the data recorded at Ny-Ålesund (78°55′30″N, 11°55′20″E) in Svalbard, Norway.

GPS observables have been used to measure the TEC, that is, the total number of electrons that are constrained in the cylinder that extends up vertically above the ground through the ionosphere. By incorporating data from multiple GPS receivers, the two-dimensional TEC maps are constructed, providing insights into the magnetosphere-ionospheric coupling (Coster et al., 2013). We use the TEC data published via the MIT Automated Processing of GPS software package (Rideout & Coster, 2006). The temporal resolution is 5 min, and the data are binned to $1° \times 1°$ grids.

The SuperDARN (Chisham et al., 2007) provides backscatter power and line-of-sight (LOS) velocity at individual radars at 1- to 2-min temporal resolution and convection maps by fitting the LOS velocity measurements. We particularly use the data from the Clyde River radar, which was located at ~5 MLT during this event.

3. Dayside Magnetosphere Transients

Figures 1a–c show ARTEMIS-C observations of IMF (panel a), solar wind velocity (b), and dynamic (cyan), plasma (red), magnetic (blue), and total (black) pressures (traces in panel c). Figures 1d–1i present MMS4 observations of (d) x (blue), y (green), and z (red) components of the magnetic field (B); (e) ion density (black) and temperature (red); (f) ion bulk velocity; (g) plasma (red) and magnetic (blue) pressures, and the sum of plasma and magnetic pressures (black); (h) current density decomposed into parallel (blue) and perpendicular (red) components to B calculated from the curlometer technique (Dunlop et al., 2002); (i) ion energy spectrogram. All the vector parameters in Figure 1 are shown in Geocentric Solar Magnetospheric (GSM) coordinates.

Over 25 min from 0742 to 0807 UT on 18 December 2017, the IMF orientation was mostly duskward and southward (Figure 1a). Before ~0751:05 UT (marked by the vertical dotted black line "C" at the top of Figure 1a) and after 0803:55 UT (marked by "D") IMF B_x component became significant, while IMF was predominantly duskward between "C" and "D." A relatively steady solar wind velocity (approximately −550 km/s; Figure 1b) suggests a transit time for the solar wind from ARTEMIS-C located at 64.2, 3.3, and 3.3 R_E to MMS4 at 8.0, −1.2, and 1.3 R_E to be ~12–13 min considering the shocked and slowed solar wind across the bow shock. A notable reduction and increase of the solar wind dynamic pressure (P_{dyn}) occurred at "C" and "D," respectively (Figure 1c). Weaker variations at ~0743:14 UT and 0746:17 UT are denoted by vertical dotted black lines, "A" (P_{dyn} increase) and "B" (P_{dyn} decrease).

These lines "A" to "D" indicate parameters of the solar wind arriving at the Earth's magnetopause when MMS made multiple magnetopause boundary layer (MLBL) crossings from 0755 UT to 0820 UT (Figures 1d–1i; "A" to "D" at the top of Figure 1d). Red, orange, light blue, and blue bars between Figures 1c and 1d indicate intervals when MMS4 observed the magnetosphere, the low-latitude boundary layer (LLBL), the MPBL, and the magnetosheath, respectively. The magnetosphere features strong and positive B_z (tens nT; Figure 1d), low density and high temperature (Figure 1e), and large fluxes of >10-keV energy ions (Figure 1i). The magnetosheath was identified by negative B_z (Figure 1d), high density and low temperature (Figure 1e), and reduction in >10-keV ion fluxes in this event (Figure 1i). In LLBL, the magnetic field is magnetospheric (i.e., positive B_z), while more magnetosheath (~hundreds to thousands eV) and weaker magnetospheric (>10 keV) plasmas coexist (Figures 1e and 1i). MPBL exhibits significantly disturbed magnetic fields with positive B_z reduced (Figure 1d) and somewhat heated plasmas of magnetosheath origin (Figures 1e and 1i).

We find the best correlation between P_{dyn} increase (decrease) and compression (expansion) of the dayside magnetosphere when assuming a ~13-min transit time from ARTEMIS-C to MMS4 (marked by dotted black lines between Figures 1c and 1d). Such deformations of the dayside magnetosphere led to relative inbound or outbound trajectories of MMS4: from the magnetosphere to LLBL corresponding to P_{dyn} increase at "A," from LLBL to the magnetosphere corresponding to P_{dyn} decrease at "B" and "C," and from MPBL to the magnetosheath, corresponding to P_{dyn} increase at "C." The short excursion to the magnetosphere at/near "B" might be also caused by the IMF change to dominant B_y and slightly positive B_z (Figure 1a).
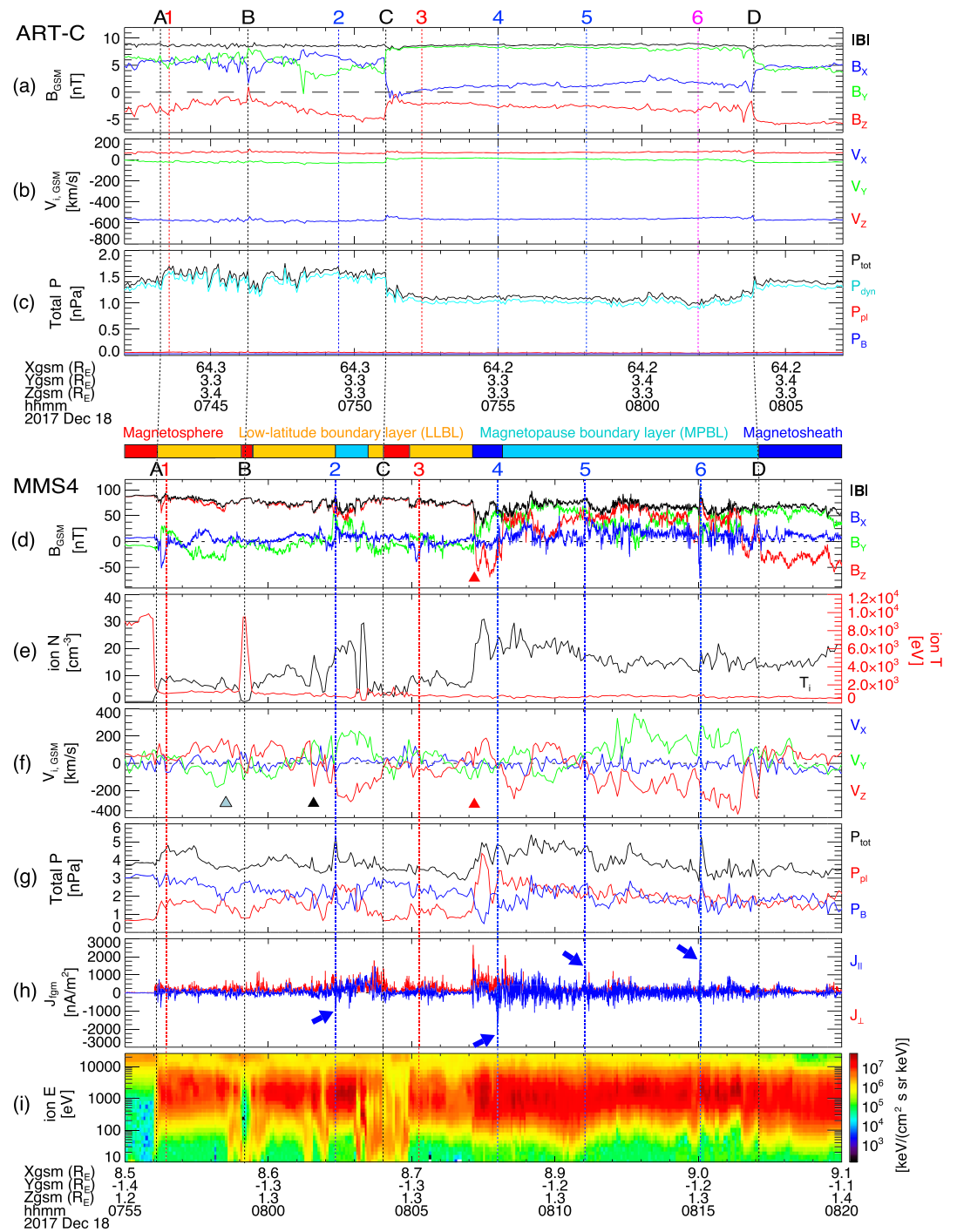
Figure 1. Upper panels (ARTEMIS-C observations of the solar wind): (a) the *x* (blue), *y* (green), and *z* (red) components of the IMF, (b) solar wind velocity, and (c) total (black profiles in panel c), dynamics (cyan), plasma (red), and magnetic (blue) pressures. Lower panels (MMS4 observations of the dayside magnetopause boundary layers): (d) *x* (blue), *y* (green), and *z* (red) components of the magnetic field (**B**); (e) ion density (black) and temperature (red); (f) ion bulk velocity; (g) plasma (red) and magnetic (blue) pressures, and the sum of plasma and magnetic pressures (black); (h) current density decomposed into parallel (blue) and perpendicular (red) components to **B** calculated from the curlometer technique (Dunlop et al., 2002); (i) ion energy spectrogram. All the vector parameters in Figure 1 are shown in geocentric solar magnetospheric (GSM) coordinates.

Toward or within the MPBL, we note a series of localized magnetic strength enhancements (e.g., vertical dashed blue lines "2," "4," "5," and "6" at the top of Figure 1d). Bipolar changes in B_x, which corresponds to B_n in this event, coincident with magnetic field enhancements suggest that these are a series of FTEs. For typical FTEs, we expect an increase in total, magnetic, and/or plasma pressures (Figure 1g), adjacent large flow velocities associated with a nearby reconnection X-line (Figure 1f), and current densities mostly parallel to **B** ($J_{||} > J\perp$) for commonly observed relatively force-free FTEs ($\mathbf{J} \times \mathbf{B} \approx 0$ (Lundquist, 1950; blue arrows in Figure 1h). Among a number of localized bipolar B_n structures observed within/across MPBL (Figure 1e), "2," "4," "5," and "6" satisfy all these predictions.

Toward or within the LLBL, a negative B_x dip followed by (weaker) positive B_x is observed at "1" and "3" (vertical dashed red lines at the top of Figure 1d). They coincide with local |**B**| enhancement (Figure 1d), increase (decrease) in the magnetic (plasma) pressure (Figure 1g), and no/little signatures in the current density (Figure 1h). These magnetic field perturbations are most likely arising from the overall motion of a southward-moving FTE drifting along the magnetopause located outward (antiearthward) from the MMS4 location.

To investigate the propagation of these FTEs or remote FTE signatures, we performed a four-spacecraft timing analysis (Paschmann & Daly, 1998; Russell et al., 1983) on each FTE/remote-FTE-signature crossing. Figure 2 presents the spacecraft configuration and separation shown in boundary normal coordinates (LMN) at/near the center of the event period (~0810:00 UT). LMN axes were determined from minimum variance analyses (Sonnerup & Scheible, 1998) using the magnetic field around 0807:10 UT (red triangle in Figure 1d) where MMS rapidly crossed the boundary from LLBL to the magnetosheath: $L = (0.07, -0.48, 0.87)$, $M = (-0.25, -0.86, -0.45)$, $N = (0.97, -0.19, -0.18)$ in GSM. N represents the direction normal to the local magnetopause, and the LM plane represents the tangential plane of the local magnetopause. The tetrahedral configuration of the four MMS spacecraft, although it was not a regular tetrahedron, provided reliable results of the timing analysis with <10% error, based on Zhou et al. (2009).
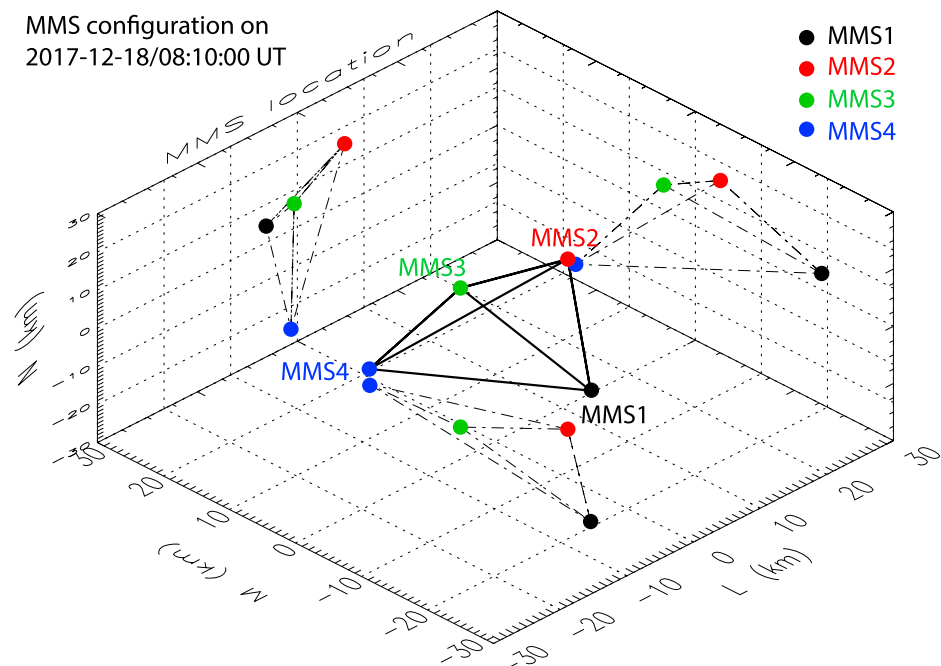
Figure 2. The configuration and separation of the four MMS spacecraft at 0810:00 UT on 17 December 2017 are shown in boundary normal coordinates (LMN). The LMN boundary normal coordinates were determined from minimum variance analyses (Sonnerup & Scheible, 1998) using the magnetic field around 08:07:10 UT (red triangle in Figure 1d). N represents the direction normal to the local magnetopause, and the LM plane represents the tangential plane of the local magnetopause.

Table 1
Normal Propagation Vectors of FTEs or FTE Signatures (Marked by Vertical Dashed red, and Blue Lines at the top of Figure 1d, '1', '2', '3', '4', '5', and '6') in GSM

	1	2	3	4	5	6
Time (UT)	~07:56:30	~08:02:17	~08:05:15	~08:08:00	~08:11:09	~08:15:05
Normal propagation in GSM	$v = 80.5$ km/s	$v = 155$ km/s	$v = 75.1$ km/s	$v = 69.9$ km/s	$v = 73.1$ km/s	$v = 224$ km/s
	(0.46, 0.86, 0.23)	(−0.31, 0.74, −0.59)	(0.15, 0.97, 0.17)	(0.28, −0.06, −0.96)	(−0.22, 0.78, −0.58)	(−0.32, 0.63, −0.71)

Table 1 lists the propagation velocities in GSM. The direction of the propagation vectors are duskward and southward for FTEs, "2," "4," "5," and "6," while remote FTE signatures, "1" and "3," propagated mainly duskward and slightly northward. The southward motion of FTEs is consistent with the common observation that B_x changes from negative to positive for these FTEs (Russell & Elphic, 1978; the slightly northward motion of remote FTE signatures, "1" and "3" will be explained in the following paragraph). This indicates that MMS was located southward of a dayside reconnection X-line. The magnitude of the propagation vectors show a wide range from ~70 to 224 km/s.

To see whether or not propagations of FTEs and remote signatures observed by MMS are consistent with predictions for the reconnected flux tube motion over the surface of a model magnetopause for specified magnetosheath and solar wind conditions (Cooling et al., 2001), we conducted runs for this model using two selected times during this event: (a) when the IMF has a significant B_{xy} component before "C," that is, (5, 5, −3) nT at ~0743:20 UT around "1" (Figure 1a) and (b) after the IMF points mostly due duskward at 0755 UT, (1, 9, −3) nT around "4" (Figure 1a). Solar wind speed and density of 550 km/s and 3 cm^{-3} together with magnetopause and bow shock standoff distances of 10 and 15 R$_E$ were used for both runs. The results for (a) and (b) are shown in Figures 3a and 3b, respectively. Both panels show the dayside magnetopause as seen from the Sun along with paths (up to 8 R$_E$ in length) of flux tubes moving northward (solid red lines) and southward (dashed blue lines) departing from different locations along a reconnection X-line. The X-line is initiated at an arbitrarily chosen location (at a point slightly northward/dawnward of the subsolar
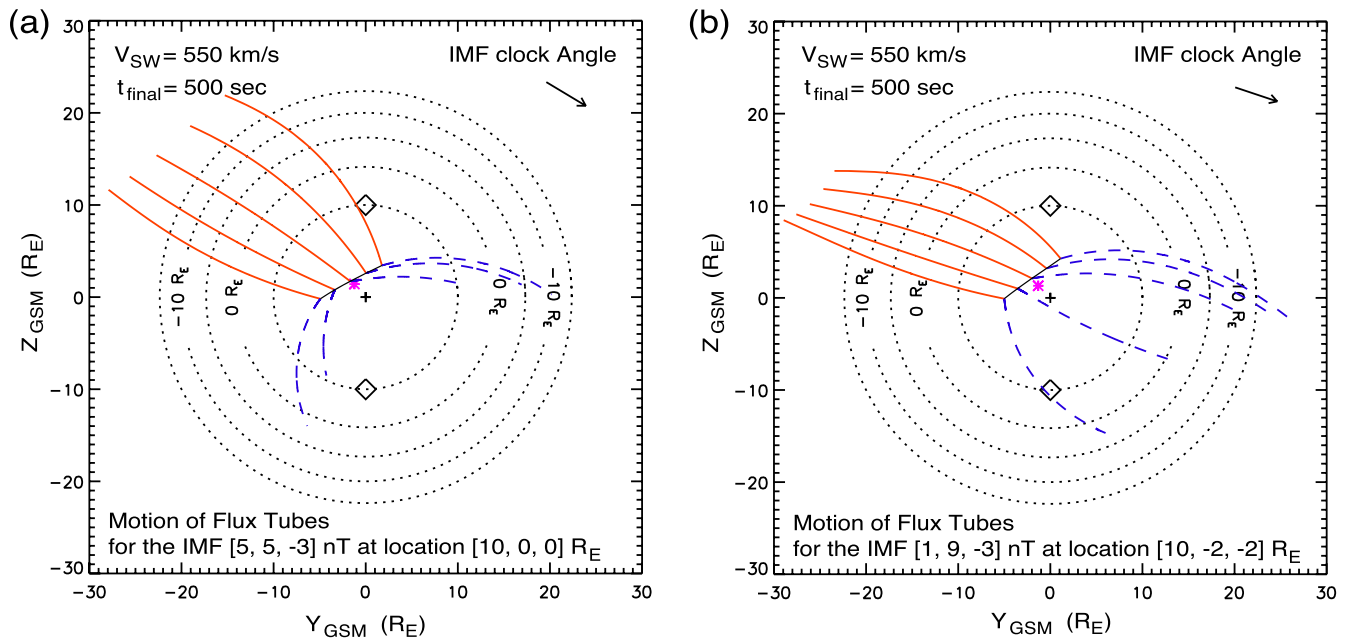
Figure 3. The propagations of FTEs predicted by Cooling et al. (2001): (a) when the IMF has a significant B_{xy} component before 'C', i.e., ((5, 5, −3) nT at ~0743:20 UT around '1' (Figures 1a) and (b) after the IMF points mostly due duskward at 0755 UT, (1, 9, −3) nT around '4' (Figure 1a). Paths of flux tubes moving northward (solid red lines) and southward (dashed blue lines) departing from different locations along a reconnection X-line are shown ~8 R$_E$ in length. The subsolar point is marked by "+." A magenta asterisk symbol indicates the MMS location on the dayside magnetopause as seen from the Sun. Two diamonds represent the location of cusps.

point in Figures 3a and 3b), but from that point it is traced perpendicular to the geomagnetic field and a draped magnetosheath field (Fear et al., 2005). The subsolar point and the location of MMS are marked by "+" and a magenta asterisk symbol, respectively. For both (a) and (b), FTEs are predicted to propagate mostly duskward across MMS. Whether they propagate southward or northward sensitively depends on the observation location with respect to the X-line: for example, FTEs at/around (a) or slightly above (b) the MMS location are predicted to drift duskward and slightly northward. The observed motion of FTEs and remote signatures (Table 1) are, thus, consistent with model predictions. The model also predicts a significant dawnward propagation of northward-moving FTEs (solid red lines) for both (a) and (b).

4. Spatiotemporal Variation of Dayside Reconnection

Within or near the LLBL (intervals indicated by orange bars at the top of Figure 1d), background B_x and B_y components (Figure 1d) fluctuated on a time scale longer than the embedded FTE/remote FTE signature, '1' or '2' or later FTEs, '3' to '6'. The bulk ion velocity also fluctuated (Figure 1f), generally from $(-V_{i,y}, +V_{i,z})$ to $(+V_{i,y}, -V_{i,z})$. Later, the $(-V_{i,y}, +V_{i,z})$ flows are seen in association with the rapid outbound crossing from LLBL to the magnetosheath (red triangle in Figure 1d) at ~0807:10 UT.

Figures 4a and 4b show the H^+ (left panels) and He^{2+} (right panels) distributions in the frame of reference where $V_\perp = 0$ for two selected times (marked by triangles in Figure 1f) during this mostly LLBL interval: (a) when $V_{i,z}$ is positive and $V_{i,y}$ is negative (light blue triangle); (b) after $V_{i,z}$ ($V_{i,z}$) changes its sign from positive to negative (negative to positive; black triangle). For each panel, the upper plot shows 2-D ($V_{||}$, $V_\perp$) distributions and the lower one shows a 1-D cut of the 2-D distributions along $V_\perp = 0$. While H^+ distributions can show mixed ions of magnetosheath or magnetosphere origin, He^{2+} distributions represent the magnetosheath population that entered the LLBL from a reconnection site. For (a), both H^+ and He^{2+} fluxes are mostly parallel (along positive $V_{||}$), indicating an X-line located south of MMS. For (b), both parallel and antiparallel populations coexist for H^+ and He^{2+}, indicating two X-lines north and south of MMS (Hasegawa et al., 2008). The antiparallel component is larger in flux than the parallel component. This difference becomes more prominent toward/after '2' when MMS was located in the MPBL where $V_{i,z}$ is significantly negative (not shown), which is similar to the multiple X-line reconnection event reported by Fuselier et al. (2018) (see figures 6 and 8 of Fuselier et al. (2018)). Figure 4c shows the H^+ distributions obtained immediately before the rapid magnetopause crossing at ~0807:10 UT (red triangle in Figures 1d and 1f) (left panel) and around the crossing (right panel). The parallel component (mostly northward jet) is dominant before the crossing, indicating an X-line located south of MMS. The jet signature becomes stronger at/around the crossing as expected for ongoing reconnection. Note that the apparently counter-streaming components in the right panel of Figure 4c are caused by a time-aliasing effect due to the B_z reversal across the magnetopause. The He^{2+} distributions during these intervals show the same features (not shown).

We also note the flow reversal from $+V_{i,z}$ to $-V_{i,z}$ around FTE '4' and FTE '5', together with no/weak jets at the center of these FTEs. This is consistent with the interpretation that the flow reversal results from two X-lines (located northward and southward of the FTE), from which outflowing jets are ejected and converge toward the FTE center (Hasegawa et al., 2010; Øieroset et al., 2011). Similarly, no/weak jets at ~0810:30 UT, where the flow reversal occurs within the MPBL are likely to be associated with MMS being located between two X-lines.

These observations, that is, the overall large-scale, longer period fluctuation in $\pm V_{i,z}$ ($\pm V_{i,y}$) (Figure 1f), reconnection jet signatures across the magnetopause, flow reversals around FTEs, and corresponding ion distribution behavior (Figure 4), therefore, indicate the spatial variation of a (dominant) X-line(s) in time, rather than repeated, complete turn-on-and-off of dayside reconnection. Considering continuously ongoing reconnection, the observed transient FTEs and remote FTE signatures, '1' to '6' are, then, likely to be associated with temporal modulation (i.e., intensification) of the reconnection rate during continuous, either a single or multiple X-line reconnection. Phan et al. (2004) and Hasegawa et al. (2016) have reported such FTEs observed during continuous magnetopause reconnection under southward IMF.

This combined continuity and transiency of dayside dynamics are consistent with ionospheric signatures of auroral brightening, which persisted during the entire period shown in Figures 1d–1i but showed an
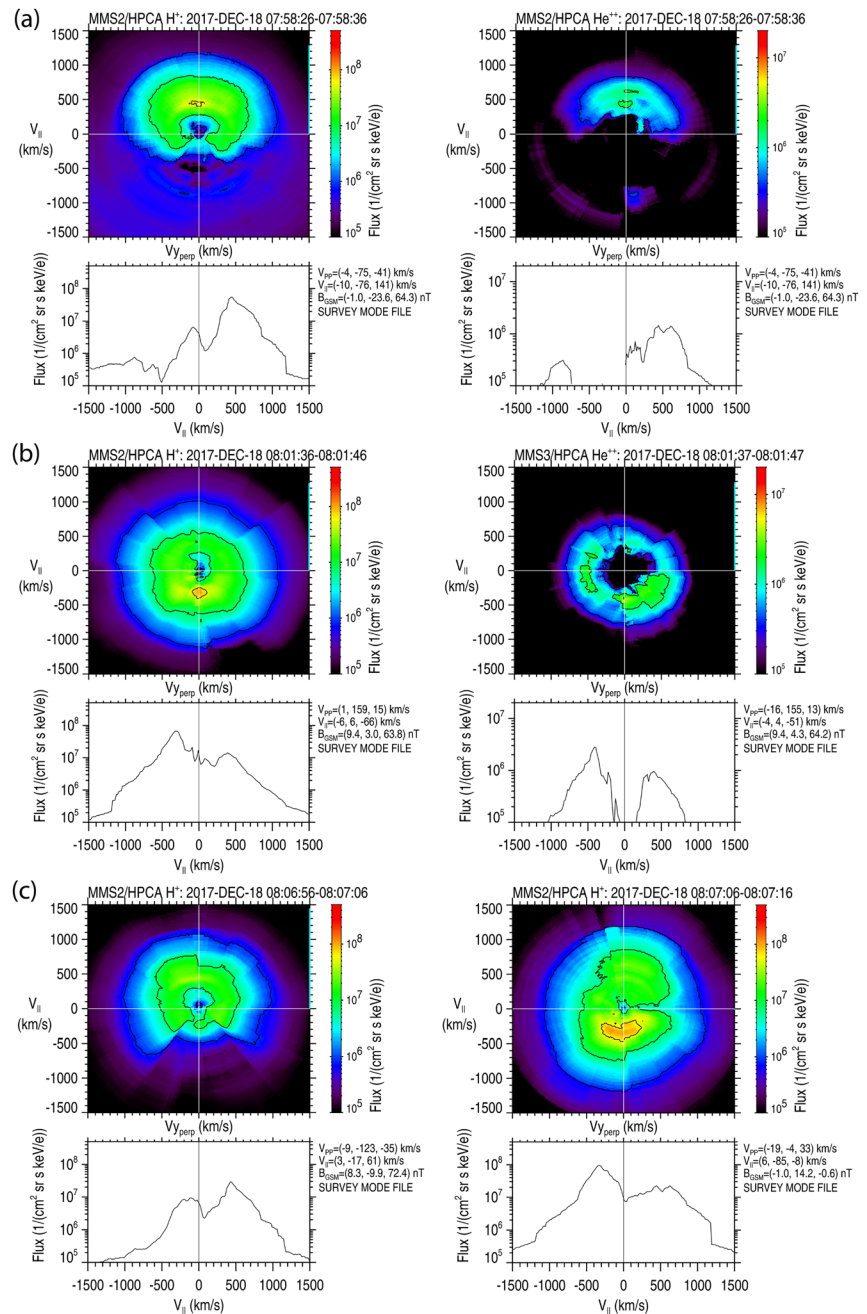
Figure 4. MMS/HPCA observations of H$^+$ (left panels) and He^{2+} (right panels) distributions in the frame of reference where $V_\perp = 0$ for two selected times (marked by triangles in Figure 1f). For each panel, the upper plot shows 2-D ($V_{||}$, $V_\perp$) distributions and the lower one shows a 1-D cut of the 2-D distributions along $V_\perp = 0$.

intensification, followed by a poleward/dawnward motion related to each of the FTEs and remote FTE signatures. We discuss detailed ionospheric responses to these dayside magnetopause activities in the following section.

5. PMAFs and TEC Associated With FTEs and Remote FTE Signatures

To quantify the extent and propagation of the ionospheric responses to the dayside transients, we investigate ASI recorded at Ny-Ålesund (78°55′30″N, 11°55′20″E) in Svalbard, Norway, near the MMS4 footprint

(77°23′56″–77°4′7″N, 14°6′47″–8°41′11″E during the interval shown in Figures 1d-i using T89). Figures 5a(A) and 5b(A) show south-to-north keograms of 630.0- and 557.7-nm wavelength emissions, respectively, from 0750 to 0930 UT. Times of MMS observations of the six FTEs and remote FTE signatures are marked at the top of Figure 5a(A) and with vertical dashed lines. Times of the expansion or compression of the dayside magnetosphere are shown at the bottom of Figures 5a(A) and 5b(A).

A series of PMAFs are identified by a few to several minute long bursts propagating northward. FTEs '1' to '6' show good correlations with PMAFs 1 to 6 as denoted by cyan arrows in Figure 5a(A). The initiation of each PMAF at ~73.5° MLAT (slightly lower initiation ALT for remote FTE signatures, '1' and '3') coincides with the times of FTE observations by MMS4 except PMAF4, which begins earlier than FTE '4'. We expect ~3-min Alfvén transit time for the effects of reconnection to propagate from the subsolar dayside reconnection site to the ionosphere along the geomagnetic field. We shift the times of MMS observations of FTEs and remote signatures by 3.5 min as shown by the vertical dashed lines in Figure 5b(A). FTEs '2', '4', '5', and '6' now well correspond to the initiation of PMAFs 4, 5, 6, and 7, while remote FTE signatures, '1' and '3' lose their ionospheric counterparts. The earlier or almost simultaneous signal arrivals at the ionosphere for the former correlation (Figure 5a(A)) may come from the possibility that the FTEs developed prior to MMS encounter with them.

In general, correlating the motion of FTEs to those of PMAFs is not straightforward due to different propagations of FTEs (Table 1 and section 5), but, more importantly, the fact that the ionospheric ends of the field lines move in response to restoring pressure balance when the magnetosphere is perturbed due to reconnection (Cowley & Lockwood, 1992), which is not exactly equivalent to the motion of the kinked magnetic field lines of FTEs. Here, we note that the intervals between FTEs, relatively consistent with those between
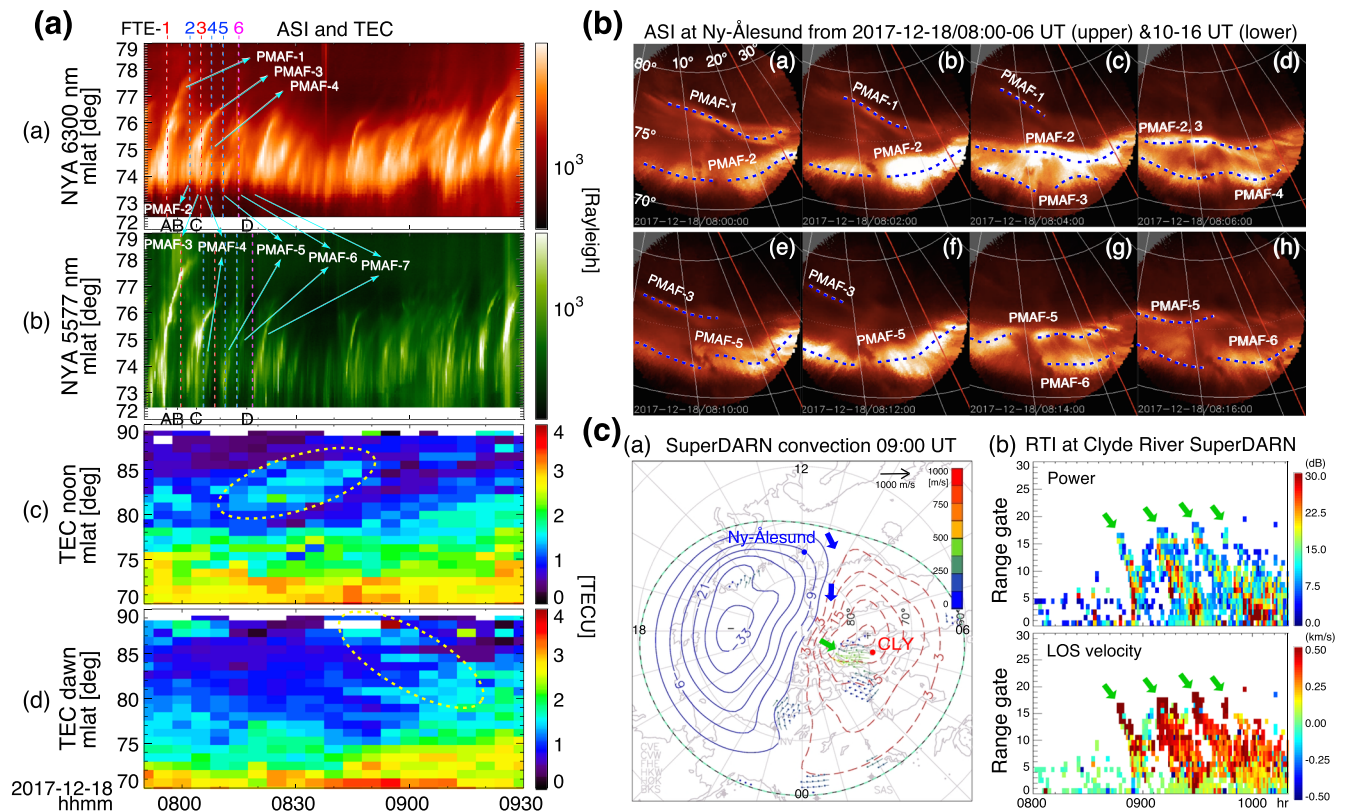
Figure 5. A. (a and b) south-to-north keograms of 630.0- and 557.7-nm wavelength ASI emissions, respectively, recorded at Ny-Ålesund (78°55′30″N, 11°55′20″E); (c and d) south-to-north keograms of median TEC measurements at the noon sector (09–15 UT) and at the dawn sector (03–09 UT). B. Times series of ASI at Ny-Ålesund during 0800–0808 UT (a–d; upper panels) and 0810–0818 UT (e–h; lower panels). C. (a) SuperDARN convection map at 0900 UT; (b) the range-time intensity (RTI) of the received power (upper panel) and line-of-sight (LOS) velocity (lower) as a function of time and range gate along beam 2 of the Clyde River SuperDARN (70.49°N and longitude −68.5°E).

PMAFs for both Figures 5a(A) and 5b(A) correlations, strongly suggest a one-to-one correspondence between dayside transients and ionospheric PMAFs. The one-to-one correspondence, in turn, supports the conjecture that the southward-moving FTEs observed by MMS and the PMAFs recorded in the Northern Hemisphere can be reasonably correlated via the assumption that a magnetopause X-line has generated FTEs simultaneously in both hemispheres, as predicted by the Cooling model (Figure 3).

We also note that the stronger signals, that is, PMAF 1, 3, and 7 occurred after/around the expansion or compression of the dayside magnetosphere, 'A', 'C', and 'D', suggestive of direct P_{dyn} effects in magnitude and extent.

Figure 5B shows a time series of ASI at Ny-Ålesund during ~0800–0806 UT (a–d; upper panels) and ~0810–0816 UT (e–h; lower panels) in (LAT, LON). We first note that auroral signatures are persistently seen at ~72–73° LAT throughout the interval during 0750–0820 UT including the period shown in Figure 5B, while an individual PMAF starts with the intensification of the auroral brightening followed by the poleward and dawnward motion (ASI movie shown in Movie S1). PMAFs are shown in blue dotted curves in Figure 5B: during 0800–0806 UT (0810–0816 UT), PMAF 1 (PMAF 3) was fading out; PMAFs 2 and 3 (PMAF 5) appeared most intense; and PMAF 4 (PMAF 6) developed. These PMAFs are found to extend over ~30° in longitude and <3° in latitude. All of them exhibit northward and westward (dawnward) motion, which is consistent with the Cooling et al. (2001) prediction (Figure 3). The location of initial brightening is relatively consistent among PMAFs at ~72–73° LAT, while PMAF 3 and PMAF 1 (indicated from Figures 5a(A) and 5b(A); Supporting Informatoin S1) initiated at lower altitudes slightly below 72° LAT. The shape of PMAF structures also displays consistency among PMAFs, in particular, between PMAFs 4 and 5, between PMAFs 2 and 6, while PMAF 3 exhibits some discrepancy (similar to PMAF 1; Supporting Information S1). This suggests that reconnection X-lines repeatedly developed in a relatively similar location on the surface of the dayside magnetopause, while inferring weak difference in the X-line location for PMAFs 1 and 3, associated with which MMS observed mostly duskward, but slightly northward propagating FTE signatures.

The decaying intensity of PMAFs has often been followed by the occurrence of polar cap patches (Carlson et al., 2004, 2006). Figures 5c(A) and 5d(A) shows south-to-north keograms of median TEC measurements at the noon sector (09–15 UT) and at the dawn sector (03–09 UT), respectively. Weak (~1.5 TECU) poleward-moving electron density enhancements (dashed ellipse in Figure 5c(A)) are shown starting at ~0820 UT after decaying of PMAFs 1 to 6. They propagate northward until ~0845 UT with a velocity of ~230 m/s, slower than the typical patch velocity. Consecutively, after 0845 UT, electron density enhancements of a similar intensity are shown at the dawn sector (dashed ellipse in Figure 5d(A)). They move dawnward at ~430 m/s until ~0915 UT.

Patches, once created, often follow the background plasma convection over the polar region. Figure 5a(C) shows the SuperDARN convection map at 0900 UT when IMF was due duskward and southward. The green arrow illustrates the dawnward flow, along which patches are likely to have propagated to the dawn sector. The patches were identified by radar at the station located in the dawn sector during this event: Figure 5b(C) shows the range-time intensity (RTI) that presents the received power (upper panel) and LOS velocity (lower) as a function of time and range gate along beam 2 of the Clyde River SuperDARN (CLY; 70.49°N and longitude −68.5°E) from 0800 UT to 1015 UT. The azimuth of the center of beam 2 is positioned at −60.4°. Each SuperDARN range gate is 45 km and range gate 0 begins 180 km from the radar. Between ~0900 and 1000 UT patch-like structures moved toward the radar (i.e., positive LOS velocities indicating motion toward the radar). This is confirmed with the apparent "downward" slant of the structures (green arrows in Figure 5b(C)). Based on the Clyde River radar location in the postmidnight/dawn sector during 0900–1000 UT (red dot in Figure 5a(C)), these structures correspond to dawnward return flows over the polar cap. The Rankin Inlet SuperDARN radar, which has a field of view (FOV) that overlaps the Clyde River radar, observed similar, but less defined patches. Therefore, it is likely that patches generated around the dayside cusp after ~0815 UT have convected across the polar cap and were observed by Clyde River at ~0900–1015 UT.

6. Summary and Conclusions

In this paper, we report the observation of solar wind-magnetosphere-ionosphere interactions using a series of FTEs observed by MMS located at the dayside MPBLs and corresponding PMAFs by ASI cameras in the

northern high-latitude ionosphere that are followed by the formation of patch-like plasma density enhancements moving poleward and then dawnward by GPS and radar. During the event, IMF was mostly duskward and southward. Although significant reduction and increase of the solar wind dynamic pressure (P_{dyn}) could result in the expansion and compression of the dayside magnetopause, the generation of the individual FTE appears less correlated with specific IMF orientation or P_{dyn} variation. As expected from the Cooling et al. (2001) model, the FTEs either propagated mostly duskward and southward or slightly northward. The model also predicted dawnward and northward-moving FTEs during this event.

Near the Northern Hemisphere MMS footprint, a series of PMAFs were observed to occur simultaneously with those FTEs. They propagated poleward and westward. The intervals between FTEs that are relatively consistent with those between PMAFs strongly suggest a one-to-one correspondence between the dayside FTEs and ionospheric PMAFs. The FTEs embedded in continuous reconnection observed by MMS and corresponding PMAFs individually occurred during persistent auroral activity recorded by ASI strongly indicate that those FTEs and PMAFs resulted from the temporal modulation of the reconnection rate during continuous reconnection, rather than the repeated, complete turn-on and turnoff of dayside reconnection.

With the decay in intensity of the PMAFs associated with the FTEs, patch-like plasma density enhancements were detected to propagate poleward and then dawnward along the background plasma convection pattern.

The sequence of these observations indicates that FTEs had led to PMAF activities (between ~0800 and 0815 UT) and PMAFs were followed by the generation of patches around the dayside cusp after ~0815 UT, and then, the patches have convected across the polar cap and reached the dawnside auroral oval at ~0910 UT. To connect southward-moving FTEs and the PMAFs and patch observations in the Northern Hemisphere, we have assumed that transient or nonsteady reconnection on a spatially extended X-line can simultaneously generate FTEs in both hemispheres. While some FTE generation mechanisms (Phan et al., 2004; Scholer, 1988; Southwood et al., 1988) simultaneously produce both northward-moving and southward-moving FTEs, other mechanisms such as a multiple sequential X-line reconnection (MSXR) model proposed by Raeder (2006) and secondary magnetic reconnection in the downstream of a dominant X-line as reported by Dong et al. (2017) may not necessarily produce FTEs on both northern and southern sides of the dominant X-line. For example, the MSXR model may have been favored for the present event that occurred on 18 December, that is, close to winter solstice. However, the near one-to-one correspondence between the FTEs observed by MMS and the PMAFs recorded in the Northern Hemisphere suggests that the FTEs in the present event more likely resulted from a nonsteady single X-line that produces FTEs in both hemispheres rather than the other mechanisms.

The extent of PMAFs is ~30° in longitude, which corresponds to ~5 R_E on the surface of the dayside magnetopause, inferring the extent of a dayside reconnection X-line. Such spatially extended X-lines on the dayside magnetopause have been reported by Dunlop et al. (2011, 2011) and Hasegawa et al. (2016) using multispacecraft conjunctions. The longitudinal and latitudinal extent of PMAFs is associated with the ionospheric footprint of FTEs, which can be related to the length and cross section of FTEs. We note that the length of FTEs can differ from the length of an X-line as FTEs can entangle nearby magnetic field lines as they drift along the magnetopause. For the present event, however, MMS was located near the subsolar point. The frequent fluctuations in the ion bulk velocity between $(-V_{i,y}, +V_{i,z})$ and $(+V_{i,y}, -V_{i,z})$ (Figure 1f) indicate a relatively close proximity of MMS to an X-line or X-lines. The PMAF signatures observed near the Northern Hemisphere MMS footprint, therefore, can be indicative of the extent of the X-line(s).

The shape and location of the initial brightening are relatively consistent among PMAFs associated with FTEs that propagated southward and duskward and are slightly different for PMAFs 1 and 3, around which FTE signatures moved mostly duskward, but slightly northward. This indicates that reconnection X-lines repeatedly developed in a relatively similar location with a similar extent on the surface of the dayside magnetopause, while inferring slight relocation/deformation for PMAFs 1 and 3.

The response time between FTEs and PMAFs is likely to be the Alfvén transit time for the effects of reconnection to propagate from the dayside reconnection site to the ionosphere along the geomagnetic field. Although the generation location of FTEs, the evolutionary phase of FTEs, and their propagation velocity might provide an accurate response time determination, the delay is mostly within a few minutes (~3.5 min in this event from Figure 5b(A) correlation). The response time between dayside FTEs (first

FTE signature) and the start and end times of a patch's transpolar transit is estimated to be ~15 and ~75 min, respectively. The 15 min might correspond to the response time for the polar cap to restore its equilibrium with the addition of newly open flux resulting from pulsed dayside reconnection (the modulation in the reconnection rate in this event) (Cowley & Lockwood, 1992; Zhang et al., 2010).

By relating the spatiotemporal variation of the driving solar wind and magnetospheric mechanism to that of the high-latitude and polar ionospheric responses, we estimated the response time and azimuthal extent of an X-line. These studies advancing the knowledge of Magnetosphere-Ionosphere-Coupling near the cusp region and in the open field line region will be supported by statistical studies via the detailed analysis techniques presented in this paper including for the different substructures of FTEs (typical force-free FTEs vs. interlinked FTEs that consist of two interlaced flux tubes (Kacem et al., 2018; Øieroset et al., 2019)), for the events of weak versus intense polar cap patches, and for a variety of solar wind inputs, which is the topic of a future study.

Data Availability Statement

MMS data sets were provided by the MMS science working group teams through the link (http//lasp.colorado.edu/mms/sdc/public/). The ARTEMIS data are available at http://themis.ssl.berkeley.edu and are supported by NASA contract NAS5-02099. The imager, TEC, and SuperDARN data are available at http://tid.uio.no/plasma/aurora/, http://cedar.openmadrigal.org/ and http://vt.superdarn.org/.

References

Amm, O., Donovan, E. F., Frey, H., Lester, M., Nakamura, R., Wild, J. A., et al. (2005). Coordinated studies of the geospaceenvironment using cluster, satellite and ground-based data: An interim review. *Annales Geophysicae*, *23*(6), 2129–2170. https://doi.org/10.5194/angeo-23-2129-2005

Angelopoulos, V. (2011). The ARTEMIS mission. *Space Science Reviews*, *165*(1-4), 3–25. https://doi.org/10.1007/s11214-010-9687-2

Burch, J. L., Moore, T. E., Torbert, R. B., & Giles, B. L. (2016). Magnetospheric Multiscale overview and science objectives. *Space Science Reviews*, *199*(1-4), 5–21. https://doi.org/10.1007/s11214-015-0164-9

Carlson, H. C. (2012). Sharpening our thinking about polar cap ionospheric patch morphology, research, and mitigation techniques. *Radio Science*, *47*, RS0L21. https://doi.org/10.1029/2011RS004946

Carlson, H. C., Moen, J., Oksavik, K., Nielsen, C. P., McCrea, I. W., Pedersen, T. R., & Gallop, P. (2006). Direct observations of injection events of subauroral plasma into the polar cap. *Geophysical Research Letters*, *33*, L05103. https://doi.org/10.1029/2005GL025230

Carlson, H. C. Jr., Oksavik, K., Moen, J., & Pedersen, T. (2004). Ionospheric patch formation: Direct measurements of the origin of a polar cap patch. *Geophysical Research Letters*, *31*, L08806. https://doi.org/10.1029/2003GL018166

Chisham, G., Lester, M., Milan, S. E., Freeman, M. P., Bristow, W. A., Grocott, A., et al. (2007). A decade of the Super Dual Auroral Radar Network (SuperDARN): Scientific achievements, new techniques and future directions. *Surveys in Geophysics*, *28*(1), 33–109. https://doi.org/10.1007/s10712-007-9017-8

Clausen, L. B. N., Moen, J. I., Hosokawa, K., & Holmes, J. M. (2016). GPS scintillations in the high latitudes during periods of dayside and nightside reconnection. *Journal of Geophysical Research: Space Physics*, *121*, 3293–3309. https://doi.org/10.1002/2015JA022199

Cooling, B. M. A., Owen, C. J., & Schwartz, S. J. (2001). Role of the magnetosheath flow in determining the motion of open flux tubes. *Journal of Geophysical Research*, *106*(A9), 18,763–18,775. https://doi.org/10.1029/2000JA000455

Coster, A., Williams, J., Weatherwax, A., Rideout, W., & Herne, D. (2013). Accuracy of GPS total electron content: GPS receiver bias temperature dependence. *Radio Science*, *48*, 190–196. https://doi.org/10.1002/rds.20011

Cowley, S. W. H., & Lockwood, M. (1992). Excitation and decay of solar-wind driven flows in the magnetosphere-ionosphere system. *Annales de Geophysique*, *10*, 103–115.

Crowley, G. (1996). Critical review of ionospheric patches and blobs. In W. R. Stone (Ed.), *Review of radio science 1993–1996*, (pp. 619–648). New York: Oxford Univ. Press.

Dong, X.-C., Dunlop, M. W., Trattner, K. J., Phan, T. D., Fu, H. S., Cao, J. B., et al. (2017). Structure and evolution of flux transfer events near dayside magnetic reconnection dissipation region: MMS observations. *Geophysical Research Letters*, *44*, 5951–5959. https://doi.org/10.1002/2017GL073411

Drury, E. E., Mende, S. B., Frey, H. U., & Doolittle, J. H. (2003). Southern Hemisphere poleward moving auroral forms. *Journal of Geophysical Research*, *108*(A3), 1114. https://doi.org/10.1029/2001JA007536

Dungey, J. W. (1961). Interplanetary magnetic field and the auroral zones. *Physical Review Letters*, *6*(2), 47–48. https://doi.org/10.1103/PhysRevLett.6.47

Dunlop, M., Balogh, A., Glassmeier, K.-H., & Robert, P. (2002). Four-point cluster application of magnetic field analysis tools: The Curlometer. *Journal of Geophysical Research*, *107*(A11), 1384. https://doi.org/10.1029/2001JA005088

Dunlop, M. W., Zhang, Q.-H., Bogdanova, Y. V., Lockwood, M., Pu, Z., Hasegawa, H., et al. (2011). Extended magnetic reconnection across the dayside magnetopause. *Physical Review Letters*, *107*(2), 025004. https://doi.org/10.1103/PhysRevLett.107.025004

Dunlop, M. W., Zhang, Q.-H., Bogdanova, Y. V., Trattner, K. J., Pu, Z., Hasegawa, H., et al. (2011). Magnetopause reconnection across wide local time. *Annales de Geophysique*, *29*(9), 1683–1697. https://doi.org/10.5194/angeo-29-1683-2011

Elphic, R. C., Lockwood, M., Cowley, S. W. H., & Sandholt, P. E. (1990). Flux transfer events at the magnetopause and in the ionosphere. *Geophysical Research Letters*, *17*(12), 2241–2244. https://doi.org/10.1029/GL017i012p02241

Fasel, G. I., Minow, J. I., Smith, R. W., Deehr, C. S., & Lee, L. C. (1992). Multiple brightenings of transient dayside auroral forms during oval expansions. *Geophysical Research Letters*, *19*(24), 2429–2432. https://doi.org/10.1029/92GL02103

Fasel, G. J. (1995). Dayside poleward moving auroral forms: A statistical study. *Journal of Geophysical Research*, *100*(A7), 11,891–11,905. https://doi.org/10.1029/95JA00854

Fear, R. C., Fazakerley, A. N., Owen, C. J., & Lucek, E. A. (2005). A survey of flux transfer events observed by cluster during strongly northward IMF. *Geophysical Research Letters*, *32*, L18105. https://doi.org/10.1029/2005GL023811

Foster, J. C. (1984). Ionospheric signatures of magnetospheric convection. *Journal of Geophysical Research*, *89*(A2), 855–865. https://doi.org/10.1029/JA089iA02p00855

Fuselier, S. A., Petrinec, S. M., Trattner, K. J., Broll, J. M., Burch, J. L., Giles, B. L., et al. (2018). Observational evidence of large-scale multiple reconnection at the Earth's dayside magnetopause. *Journal of Geophysical Research: Space Physics*, *123*, 8407–8421. https://doi.org/10.1029/2018JA025681

Goodwin, L., Iserhienrhien, B., Miles, D. M., Patra, S., van der Meeren, C., Buchert, S. C., et al. (2015). Swarm in situ observations of *F*-region polar cap patches created by cusp precipitation. *Geophysical Research Letters*, *42*, 996–1003. https://doi.org/10.1002/2014GL062610

Hasegawa, H., Kitamura, N., Saito, Y., Nagai, T., Shinohara, I., Yokota, S., et al. (2016). Decay of mesoscale flux transfer events during quasi-continuous spatially extended reconnection at the magnetopause. *Geophysical Research Letters*, *43*, 4755–4762. https://doi.org/10.1002/2016GL069225

Hasegawa, H., Retino, A., Vaivads, A., Khotyaintsev, Y., Nakamura, R., Takada, T., et al. (2008). Retreat and reformation of X-line during quasi-continuous tailward-of-the-cusp reconnection under northward IMF. *Geophysical Research Letters*, *35*, L15104. https://doi.org/10.1029/2008GL034767

Hasegawa, H., Wang, J., Dunlop, M. W., Pu, Z. Y., Zhang, Q. H., Lavraud, B., et al. (2010). Evidence for a flux transfer event generated by multiple X-line reconnection at the magnetopause. *Geophysical Research Letters*, *37*, L16101. https://doi.org/10.1029/2010GL044219

Hwang, K.-J., Dokgo, K., Choi, E., Burch, J. L., Sibeck, D. G., Giles, B. L., et al. (2020). Magnetic reconnection inside a flux rope induced by Kelvin-Helmholtz vortices. *Journal of Geophysical Research: Space Physics*, *125*, e2019JA027665. https://doi.org/10.1029/2019JA027665

Hwang, K.-J., Sibeck, D. G., Burch, J. L., Choi, E., Fear, R. C., Lavraud, B., et al. (2018). Small-scale flux transfer events formed in the reconnection exhaust region between two X lines. *Journal of Geophysical Research: Space Physics*, *123*, 8473–8488. https://doi.org/10.1029/2018JA025611

Hwang, K.-J., Sibeck, D. G., Giles, B. L., Pollock, C. J., Gershman, D., Avanov, L., et al. (2016). The substructure of a flux transfer event observed by the MMS spacecraft. *Geophysical Research Letters*, *43*, 9434–9443. https://doi.org/10.1002/2016GL070934

Hwang, K.-J., Dokgo K., Choi E., Burch J. L., Sibeck D. G., Giles B. L., et al. (2020). Magnetic Reconnection Inside a Flux Rope Induced by Kelvin-Helmholtz Vortices. *Journal of Geophysical Research: Space Physics*, *125*(4). https://doi.org/10.1029/2019ja027665

Kacem, I., Jacquey, C., Génot, V., Lavraud, B., Vernisse, Y., Marchaudon, A., et al. (2018). Magnetic reconnection at a thin current sheet separating two interlaced flux tubes at the Earth's magnetopause. *Journal of Geophysical Research: Space Physics*, *123*, 1779–1793. https://doi.org/10.1002/2017JA024537

Knudsen, W. C. (1974). Magnetospheric convection and the high-latitude F_2 ionosphere. *Journal of Geophysical Research*, *79*(7), 1046–1055. https://doi.org/10.1029/JA079i007p01046

Lee, L. C., & Fu, Z. F. (1985). A theory of magnetic flux transfer at the Earth's magnetopause. *Geophysical Research Letters*, *12*(2), 105–108. https://doi.org/10.1029/GL012i002p00105

Lockwood, M., & Carlson, H. C. (1992). Production of polar cap electron density patches by transient magnetopause reconnection. *Geophysical Research Letters*, *19*(17), 1731–1734. https://doi.org/10.1029/92GL01993

Lockwood, M., Sandholt, P. E., & Cowley, S. W. H. (1989). Dayside auroral activity and magnetic flux transfer from the solar wind. *Geophysical Research Letters*, *16*(1), 33–36. https://doi.org/10.1029/GL016i001p00033

Lorentzen, D. A., Moen, J., Oksavik, K., Sigernes, F., Saito, Y., & Johnsen, M. G. (2010). In situ measurement of a newly created polar cap patch. *Journal of Geophysical Research*, *115*, A12323. https://doi.org/10.1029/2010JA015710

Lundquist, S. (1950). Magnetohydrostatic fields. *Arkiv foer Physik*, *2*, 361–365.

McWilliams, K. A., Yeoman, T. K., & Provan, G. (2000). A statistical survey of dayside pulsed ionospheric flows as seen by the CUTLASS Finland HF radar. *Annales de Geophysique*, *18*(4), 445–453. https://doi.org/10.1007/s005850050902

McWilliams, K. A., Yeoman, T. K., Sibeck, D. G., Milan, S. E., Sofko, G. J., Nagai, T., et al. (2004). Simultaneous observations of magnetopause flux transfer events and of their associated signatures at ionospheric altitudes. *Annales Geophysicae*, *22*(6), 2181–2199. https://doi.org/10.5194/angeo-22-2181-2004

Milan, S. E., Lester, M., Cowley, S. W. H., Moen, J., Sandholt, P. E., & Owen, C. J. (1999). Meridian-scanning photometer, coherent HF radar, and magnetometer observations of the cusp: A case study. *Annales Geophysicae*, *17*(2), 159–172. https://doi.org/10.1007/s00585-999-0159-5

Moen, J., Carlson, H. C., Rinne, Y., & Skjæveland, Å. (2012). Multi-scale features of solar terrestrial coupling in the cusp ionosphere. *Journal of Atmospheric and Solar - Terrestrial Physics*, *87-88*, 11–19. https://doi.org/10.1016/j.jastp.2011.07.002

Neudegg, D. A., Cowley, S. W. H., McWilliams, K. A., Lester, M., Yeoman, T. K., Sigwarth, J., et al. (2001). The UV aurora and ionospheric flows during flux transfer events. *Annales Geophysicae*, *19*(2), 179–188. https://doi.org/10.5194/angeo-19-179-2001

Neudegg, D. A., Cowley, S. W. H., Milan, S. E., Yeoman, T., Lester, M., Provan, G., et al. (2000). A survey of magnetopause FTEs and associated flow bursts in the polar ionosphere. *Annales Geophysicae*, *18*(4), 416–435. https://doi.org/10.1007/s00585-000-0416-0

Nishimura, Y., Lyons, L. R., Zou, Y., Oksavik, K., Moen, J. I., Clausen, L. B., et al. (2014). Day-night coupling by a localized flow channel visualized by polar cap patch propagation. *Geophysical Research Letters*, *41*, 3701–3709. https://doi.org/10.1002/2014GL060301

Øieroset, M., Phan, T. D., Drake, J. F., Eastwood, J. P., Fuselier, S. A., Strangeway, R. J., et al. (2019). Reconnection with magnetic flux pileup at the interface of converging jets at the magnetopause. *Geophysical Research Letters*, *46*, 1937–1946. https://doi.org/10.1029/2018GL080994

Øieroset, M., Phan, T. D., Eastwood, J. P., Fujimoto, M., Daughton, W., Shay, M. A., et al. (2011). Direct evidence for a three-dimensional magnetic flux rope flanked by two active magnetic reconnection X lines at Earth's magnetopause. *Physical Review Letters*, *107*(16), 165,007. https://doi.org/10.1103/PhysRevLett.107.165007

Paschmann, G., & Daly, P. W. (1998). Analysis methods for multispacecraft data, Sci. Rep. 001, Int. Space Sci. Inst., Bern.

Phan, T. D., Dunlop, M. W., Paschmann, G., Klecker, B., Bosqued, J. M., Rème, H., et al. (2004). Cluster observations of continuous reconnection at the magnetopause under steady interplanetary magnetic field conditions. *Annales de Geophysique*, *22*(7), 2355–2367. https://doi.org/10.5194/angeo-22-2355-2004

Pinnock, M., Rodger, A. S., Dudeney, J. R., Baker, K. B., Newell, P. T., Greenwald, R. A., & Greenspan, M. E. (1993). Observations of an enhanced convection channel in the cusp ionosphere. *Journal of Geophysical Research*, *98*(A3), 3767–3776. https://doi.org/10.1029/92JA01382

Pinnock, M., Rodger, A. S., Dudeney, J. R., Rich, F., & Baker, K. B. (1995). High spatial and temporal resolution observations of the ionospheric cusp. *Annales Geophysicae*, *13*(9), 919–925. https://doi.org/10.1007/s00585-995-0919-9

Pollock, C., Moore, T., Jacques, A., Burch, J., Gliese, U., Saito, Y., et al. (2016). Fast plasma investigation for Magnetospheric Multiscale. *Space Science Reviews*, *199*(1-4), 331–406. https://doi.org/10.1007/s11214-016-0245-4

Provan, G., & Yeoman, T. K. (1999). Statistical observations of the MLT, latitude and size of pulsed ionospheric flows with the CUTLASS Finland radar. *Annales Geophysicae*, *17*(7), 855–867. https://doi.org/10.1007/s00585-999-0855-1

Provan, G., Yeoman, T. K., & Cowley, S. W. H. (1999). The influence of the IMF by component on the location of pulsed flows in the dayside ionosphere observed by an HF radar. *Geophysical Research Letters*, *26*(4), 521–524. https://doi.org/10.1029/1999GL900009

Rae, I. J., Fenrich, F. R., Lester, M., McWilliams, K. A., & Scudder, J. D. (2004). Solar wind modulation of cusp particle signatures and their associated ionospheric flows. *Journal of Geophysical Research*, *109*, A03223. https://doi.org/10.1029/2003JA010188

Raeder, J. (2006). Flux transfer events: 1. Generation mechanism for strong southward IMF. *Annales de Geophysique*, *24*(1), 381–392. https://doi.org/10.5194/angeo-24-381-2006

Rideout, W., & Coster, A. (2006). Automated GPS processing for global total electron content data. *GPS Solutions*, *10*(3), 219–228. https://doi.org/10.1007/s10291-006-0029-5

Russell, C. T., Anderson, B. J., Baumjohann, W., Bromund, K. R., Dearborn, D., Fischer, D., et al. (2014). The Magnetospheric Multiscale magnetometers. *Space Science Reviews*, *199*(1-4), 189–256. https://doi.org/10.1007/s11214-014-0057-3

Russell, C. T., & Elphic, R. C. (1978). Initial ISEE magnetometer results—Magnetopause observations. *Space Science Reviews*, *22*(6), 681–715. https://doi.org/10.1007/BF00212619

Russell, C. T., Mellott, M. M., Smith, E. J., & King, J. H. (1983). Multiple spacecraft observations of interplanetary shocks: Four spacecraft determination of shock normals. *Journal of Geophysical Research*, *88*(A6), 4739. https://doi.org/10.1029/JA088iA06p04739

Sandholt, P. E., Deehr, C. S., Egeland, A., Lybekk, B., Viereck, R., & Romick, G. J. (1986). Signatures in the dayside aurora of plasma transfer from the magnetosheath. *Journal of Geophysical Research*, *91*(A9), 10,063–10,079. https://doi.org/10.1029/JA091iA09p10063

Sandholt, P. E., Farrugia, C. J., Denig, W. F., Cowley, S. W. H., & Lester, M. (2003). Spontaneous and driven cusp dynamics: Optical aurora, particle precipitation, and plasma convection. *Planetary and Space Science*, *51*(12), 797–812. https://doi.org/10.1016/S0032-0633(03)00114-4

Scholer, M. (1988). Magnetic flux transfer at the magnetopause based on single X-line bursty reconnection. *Geophysical Research Letters*, *15*(4), 291–294. https://doi.org/10.1029/GL015i004p00291

Scholer, M. (1995). Models of flux transfer events. In P. Song, B. U. Ö. Sonnerup, & M. F. Thomsen (Eds.), *Physics of the Magnetopause*, *Geophys. Monogr. Ser.*, (Vol. 90, pp. 235–245). Washington, D. C: American Geophysical Union.

Sonnerup, B. U. Ö., & Scheible, M. (1998). Minimum and maximum variance analysis. *ISSI Scientific Report*, *1*, 185–220.

Southwood, D. J., Farrugia, C. J., & Saunders, M. A. (1988). What are flux transfer events? *Planetary and Space Science*, *36*(5), 503–508. https://doi.org/10.1016/0032-0633(88)90109-2

Walsh, B. M., Komar, C. M., & Pfau-Kempf, Y. (2017). Spacecraft measurements constraining the spatial extent of a magnetopause reconnection X line. *Geophysical Research Letters*, *44*, 3038–3046. https://doi.org/10.1002/2017GL073379

Wang, B., Nishimura, Y., Lyons, L. R., Zou, Y., Carlson, H. C., Frey, H. U., & Mende, S. B. (2016). Analysis of close conjunctions between dayside polar cap airglow patches and flow channels by all-sky imager and DMSP. *Earth Planet Space*, *68*(1), 150. https://doi.org/10.1186/s40623-016-0524-z

Weber, E. J., & Buchau, J. (1981). Polar cap *F*-layer auroras. *Geophysical Research Letters*, *8*(1), 125–128. https://doi.org/10.1029/GL008i001p00125

Wild, J. A., Cowley, S. W. H., Davies, J. A., Khan, H., Lester, M., Milan, S. E., et al. (2001). First simultaneous observations of flux transfer events at the high-latitude magnetopause by the cluster spacecraft and pulsed radar signatures in the conjugate ionosphere by the CUTLASS and EISCAT radars. *Annales Geophysicae*, *19*(10/12), 1491–1508. https://doi.org/10.5194/angeo-19-1491-2001

Wild, J. A., Milan, S. E., Cowley, S. W. H., Dunlop, M. W., Owen, C. J., Bosqued, J. M., et al. (2003). Coordinated interhemispheric SuperDARN radar observations of the ionospheric response to flux transfer events observed by the cluster spacecraft at the high-latitude magnetopause. *Annales Geophysicae*, *21*(8), 1807–1826. https://doi.org/10.5194/angeo-21-1807-2003

Wild, J. A., Milan, S. E., Davies, J. A., Cowley, S. W. H., Carr, C. M., & Balogh, A. (2005). Double star, cluster, and ground-based observations of magnetic reconnection during an interval of duskward oriented IMF: Preliminary results. *Annales Geophysicae*, *23*(8), 2903–2907. https://doi.org/10.5194/angeo-23-2903-2005

Wild, J. A., Milan, S. E., Davies, J. A., Dunlop, M. W., Wright, D. M., Carr, C. M., et al. (2007). On the location of dayside magnetic reconnection during an interval of duskward oriented IMF. *Annales Geophysicae*, *25*(1), 219–238. https://doi.org/10.5194/angeo-25-219-2007

Young, D. T., Burch, J. L., Gomez, R. G., De Los Santos, A., Miller, G. P., Wilson, P., et al. (2014). Hot plasma composition analyzer for the Magnetospheric Multiscale mission. *Space Science Reviews*, *199*(1–4), 407–470. https://doi.org/10.1007/s11214-014-0049-6

Zhang, Q.-H., Dunlop, M. W., Lockwood, M., Liu, R. Y., Hu, H. Q., Yang, H. G., et al. (2010). Simultaneous observations of reconnection pulses at cluster and their effects on the cusp aurora observed at the Chinese Yellow River Station. *Journal of Geophysical Research*, *115*, A10237. https://doi.org/10.1029/2010JA015526

Zhou, X.-Z., Pu, Z. Y., Zong, Q.-G., Song, P., Fu, S. Y., Wang, J., & Zhang, H. (2009). On the error estimation of multi-spacecraft timing method. *Annals of Geophysics*, *27*(10), 3949–3955. https://doi.org/10.5194/angeo-27-3949-2009